



Article

Seismic Response of a Liquefiable Site-Underground Structure System

Xinjun Cheng ^{1,2,3,*} , Xiang Xu ², Zhinan Hu ¹, Liping Jing ³ , Haian Liang ³ and Jie Cui ⁴

¹ State Key Laboratory of Mechanical Behavior and System Safety of Traffic Engineering Structures, Shijiazhuang Tiedao University, Shijiazhuang 050043, China

² School of Civil and Architectural Engineering, East China University of Technology, Nanchang 330013, China

³ Key Laboratory of Earthquake Engineering and Engineering Vibration, Institute of Engineering Mechanics, China Earthquake Administration, Harbin 150080, China

⁴ School of Civil Engineering, Guangzhou University, Guangzhou 510006, China

* Correspondence: chengxinjuniem@163.com

Abstract: To study the dynamic response of a saturated sand-underground structure system subjected to earthquakes, a series of shaking table tests with a geometric scale ratio of 1/30 were conducted. Based on the experimental acceleration records of testing soil deposits, the relationship between dynamic shear stress and horizontal soil displacement was analyzed by the 1D shear beam inverse calculation method. Meanwhile, the development law of the equivalent dynamic horizontal subgrade reaction coefficient and the dynamic strain of the sidewall in the underground structure has also been discussed. The testing results indicate that the dynamic shear stress of the soil deposit under the bottom plate of the underground structure is larger than that of the soils surrounding the sidewall and above the roof plate; in addition, the soil displacement tends to decrease with the buried depth. The dynamic shear stress–displacement hysteretic loop of the soil deposits tends to be plump as the input amplitude increases. The spectral characteristics of ground motions obviously influence both the dynamic shear stress–displacement hysteretic curve and the excess pore water pressure ratio of saturated sand soil, especially under medium and strong excitations. The equivalent dynamic horizontal subgrade reaction coefficient decreases with the increase of soil depth, and the difference between the coefficient above and underneath the underground structure model can reach 7.589 MN/m³. On the contrary, the equivalent dynamic horizontal subgrade reaction coefficient decreases with the increase of the input amplitude of ground motions, and the maximum reduction ratios of the coefficient are 74.4%, 66.7%, and 47.3%, corresponding to the El-Centro, Kobe, and Wulong ground motions, respectively. The soil liquefaction has a certain effect on the equivalent dynamic horizontal subgrade reaction coefficient. In general, the dynamic strain at the top of the sidewall in the underground structure is higher than that at the bottom of the sidewall, which illustrates that the deformation of underground structures is in good agreement with the seismic deformation mode of soil deposits.

Keywords: seismic performance; underground structures; seismic damage; shaking table test; soil site



Citation: Cheng, X.; Xu, X.; Hu, Z.; Jing, L.; Liang, H.; Cui, J. Seismic Response of a Liquefiable Site-Underground Structure System. *Buildings* **2022**, *12*, 1751. <https://doi.org/10.3390/buildings12101751>

Academic Editors: Chunfeng Zhao, Xiaohui Yu and Wen Bai

Received: 26 September 2022

Accepted: 17 October 2022

Published: 20 October 2022

Publisher's Note: MDPI stays neutral with regard to jurisdictional claims in published maps and institutional affiliations.



Copyright: © 2022 by the authors. Licensee MDPI, Basel, Switzerland. This article is an open access article distributed under the terms and conditions of the Creative Commons Attribution (CC BY) license (<https://creativecommons.org/licenses/by/4.0/>).

1. Introduction

The large-scale construction of the urban rail transport system and rapid urbanization in China has captured worldwide attention. In addition, more and more underground engineering structures have been constructed in alluvial plains, rivers, and even oceans. However, earthquake-induced soil liquefaction can lead to the uneven ground settlement and adverse deformation, which may be detrimental to the underground engineering structures embedded in saturated sand ground. Thus, soil liquefaction is obviously a threat.

Soil liquefaction is usually regarded as one of the crucial causes of fatal damages of underground structures. To investigate the effects of the soil liquefaction on the foundation–subway station interaction, Wang et al. [1] conducted a large-scale shaking table test to

investigate the dynamic interaction between the foundation and the subway station. The testing results showed that the liquefaction state of surrounding soil significantly changed the interaction mode between the foundation and the subway station.

How to reveal the seismic behavior of liquefiable soil is important to the anti-seismic safety of underground structures. Scholars have carried out relevant research about this problem. Based on a simplified soil hysteresis model for one-dimensional analysis of site seismic behavior and Biot's dynamic consolidation theory, Zhao et al. [2] mainly studied the relationship of the pore water pressure and the soil skeleton volumetric deformation, and then improved the soil model. Their research indicated that the nonlinear features of the liquefiable site would be captured by the improved soil model. Considering the data of the shaking table test of liquefiable soil using a huge laminar shear box and the input motion of the 1999 Chi-Chi earthquake record, the variation of soil mechanical behaviors during earthquake events was then investigated by Ko et al. [3]. They also deduced the stress–strain relationship of the testing soil. The research findings are beneficial to calculate adequate soil parameters during the anti-seismic design of underground structures. Accurate calculation of the dynamic parameters of the liquefiable soil, i.e., shear modulus, damping ratios, and effective stress, are the crucial criteria for the estimation of foundation problems and the seismic performance of underground structures. Chattaraj et al. [4] studied the dynamic features of the Kasai River sand by conducting the resonant column tests and undrained cyclic triaxial tests. They also proposed a new correlation of dynamic shear damping and shear modulus. To study the influence mechanisms of earthquake histories on the liquefaction resistance of a liquefied sand site, Ye et al. [5] conducted centrifuge table tests. The testing results indicated that the seismic histories had complex effects on sand liquefaction resistance. Xie et al. [6] assessed sand re-liquefaction resistance by using repeated centrifuge shaking table model tests and a micro-image acquisition system. The testing results also suggested that the effects of the excess pore pressure dissipation on the testing sand deposit must be considered in evaluating sand re-liquefaction resistance. Shooshpasha et al. [7] conducted dynamic investigations based on a fully nonlinear, elastoplastic coupled stress flow method. They proposed that the soil deformation mode as well as the excess pore water pressure should be considered to evaluate liquefaction potential, since the silty sand soil deposit underlying the surcharge may be liquefied, and thus can cause large deformations.

Since the 1995 Kobe earthquake, the influence of earthquakes on underground structures has drawn the attention of scholars. The stability state of surrounding soils of underground structures is an important factor to the seismic response of underground structures. Seismic damages of underground structures have been frequently discovered in previous earthquakes, especially in saturated sand deposits [8–12]. To study the seismic deformation mode of underground structures in a liquefiable site, Zhuang et al. [13] revised an existing sand model and implanted it into the finite element method software. Then, the seismic performance of a large-scale metro station built in liquefiable ground was investigated by numerical simulation. Their study indicated that the existing metro station influenced the liquefaction of the nearby sand deposits. Based on an overall time history numerical method, Chen et al. [14] analyzed the dynamic interaction of the nearby soils and an underground station built in a slightly sloping liquefiable site. They pointed out that the rotation and the asymmetrical dynamic damage of the station in a slightly sloping liquefiable site need attention. Zhao et al. [15] proposed a fully coupled, nonlinear effective stress analysis framework for better understanding of the seismic features of an immersed tunnel-seabed system. They pointed out that ignoring the seabed liquefaction and environment loads during the structural design process can be misleading. Li et al. [16,17] developed a fully fluid–solid coupling model to investigate the dynamic responses of underground structures in saturated soil deposits and found that the dynamic responses of the tunnel seemed to be underestimated by using the single-phase medium model. The studies mentioned above indicate that a full understanding of the seismic performance of saturated sand is necessary for the seismic estimation of underground structures.

Nowadays, underground structures are becoming an indispensable part of the effective transportation and environmental means of offering underground infrastructure. In consideration of the seismic safety of underground structures, the research method is also an important factor for seismic analysis of underground structures. Yu et al. [18,19] estimated the dynamic responses of a long tunnel structure by conducting a series of multi-point shaking table tests. Their experimental results demonstrated that the acceleration observed from the tunnel structure was larger than that obtained from the surrounding soil. The effects of non-uniform earthquakes should be noticed during the anti-seismic design of super-long underground structures. To investigate the seismic performances of underground structures in coral, Ding et al. [20] carried out a series of shaking table tests. The dynamic test results revealed that the increasing groundwater level influenced the excess pore pressure of the coral sand and the settlement of the tunnel. Kheradi et al. [21] launched numerical simulations and 1 g shaking table tests to estimate the anti-seismic performances of shallow buried box culverts. Based on the testing results and simulation reports, an optimum means for box culverts was proposed. Chen et al. [22] carried out a series of dynamic tests for an irregular cross-section subway constructed in soft soil ground, and the testing results introduced that the low-frequency band concentration and amplification effects can be reflected by the spectral characteristics of the liquefied sand soil deposit. Given that the enclosure structure is a fundamental part of the prefabricated subway station structure (PSSS) system, Tao et al. [23] introduced the dynamic strains, acceleration values, and joint deformations of a PSSS by conducting shaking table tests. Tao revealed that the enclosure structure can efficiently enhance the anti-deformation capacity and joint stiffness of the whole PSSS. To investigate the soil deposit uplift effects on underground tunnels, Koseki [24] conducted a variety of experimental tests. Koseki found that deformations of the soil surrounding the sidewall influenced the seismic deformation of a completely buried box-type structure. Zhu et al. [25] evaluated the effectiveness of four kinds of simplified pseudo-static methods for the dynamic performance analysis of underground structures. The disadvantage of the simplified pseudo-static methods is they neglect the temporal and spatial variability of the sandy soil–tunnel structure interaction. Mahmoud et al. [26] explored the seismic performance of an underground structure constructed in sandy soil deposits by using the finite differences method. It was found that setting gravel drains around the tunnel structure as well as an impermeable layer under the underground structure can efficiently prevent the structural uplift.

As there is an increasing number of underground construction activities in the complex water environment, it is necessary to investigate the dynamic behavior of saturated sand soil as well as its effects on the seismic response of underground structures. However, the seismic behavior, especially the hysteretic performance of saturated sand soil, and its effects on underground structures is deficient. Thus, the claim of a comprehensive awareness of the hysteretic behavior of sandy soils acquires importance. To gain a full understanding of the shear stress time history and horizontal deformation of saturated sand soil and ascertain the effect of the soil foundation on the dynamic strain of underground structures, a series of shaking table tests were conducted. Based on the shaking table tests for saturated sand soil, the excess pore water pressure ratio, the hysteretic behavior of the soil with different buried depths, the equivalent dynamic horizontal subgrade reaction coefficient (based on a calculation method on the basis of shear stress–displacement hysteretic curves of saturated sand), and the peak dynamic strain values of an underground structure embedded in the liquefiable site were comprehensively investigated in this study. The flowchart regarding the whole research process is shown in Figure 1.

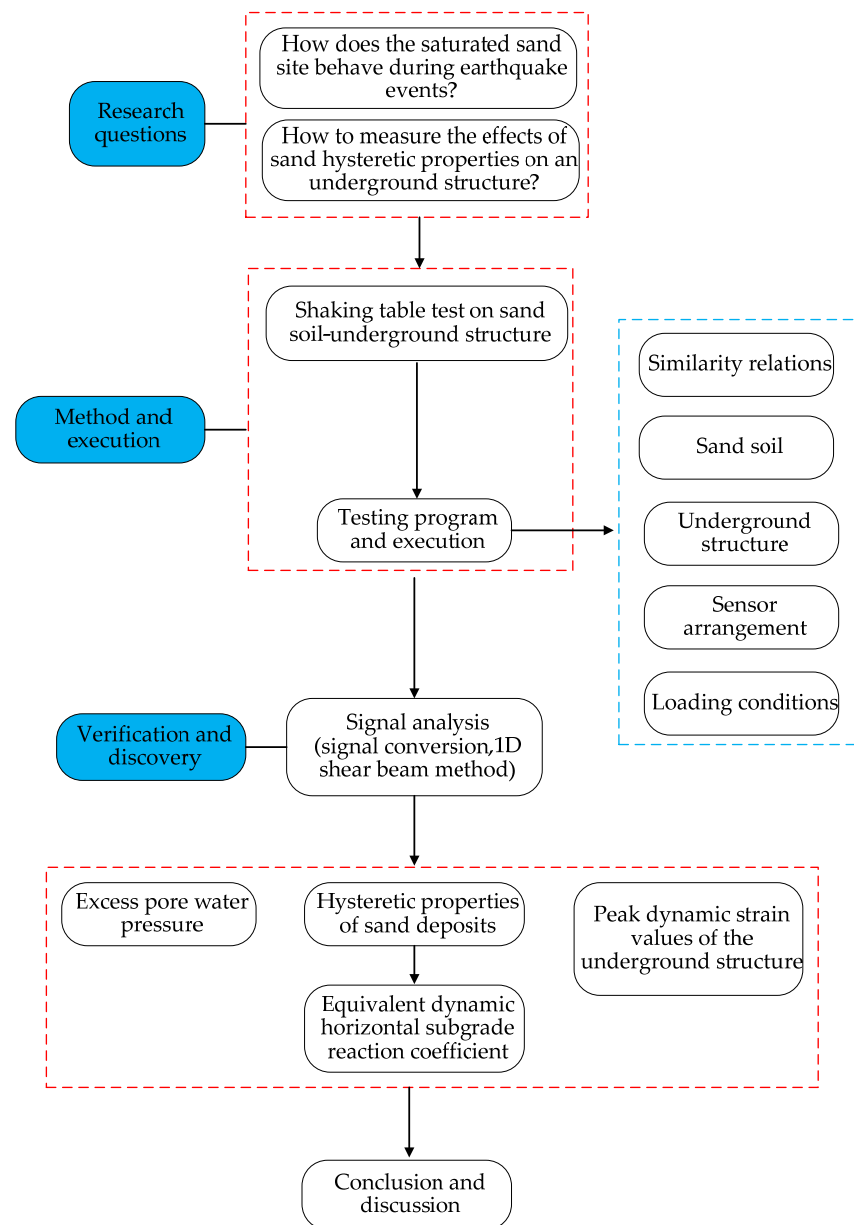


Figure 1. Research roadmap.

2. Testing Program

The shaking table test was conducted in the key laboratory of earthquake engineering and engineering vibration, institute of engineering mechanics, China earthquake administration. As for the shaking table, the size is 5 by 5 m, the ultimate load-bearing capacity is 30 tons, and the maximum horizontal and vertical displacements are ± 80 and ± 50 mm, respectively. Both the ultimate horizontal and vertical acceleration are 1 g. The frequency ranges from 0.5 to 40 Hz.

The testing program mainly includes the design scheme of the similarity ratio, the fabrication of the structural model, the selection of the foundation soil and model box, and the design of loading conditions.

2.1. Similarity Ratio

Considering the bearing capacity of the shaking table and the size of the laminar shear model box independently developed by the research group, a 1/30 geometric similarity ratio was adopted for the test. According to the law of Buckingham and previous studies

about dynamic similarity [27–29], a geometry length, L , an equivalent density of ρ_e , and an elastic modulus, E , were characterized as fundamental physical quantities. An elastic modulus of 7880 N/mm² of a prismoid made of the testing particle–concrete has been exhibited, which also presented a similarity ratio to that of the prototype C35 concrete, where the ratio was 1/4. The main dynamic similarity values between the testing model and the prototype are listed in Table 1. It should be noted that the similitude ratio of the equivalent density is related to the mass of the structure model M_M , the similitude ratio S_L , the mass of counterweight blocks M_A , and the mass of the structure prototype M_P . After a comprehensive consideration of the bearing capacity of the shaking table and the space of the testing underground structure model, the similitude ratio of equivalent density was taken as 1.875.

Table 1. Similitude relations of the model structure.

Physical Quantities	Similitude Relations	Model Structure
Length	S_L	1/30
Displacement	$S_\delta = S_L$	1/30
Equivalent density	$S_{\rho_e} = (M_M + M_A)S_L^{-3}/M_P$	1.875
Duration	$S_T = S_L\sqrt{S_{\rho_e}/S_E}$	1/4
Elastic modulus	S_E	1/4
Acceleration	$S_a = S_E/(S_LS_{\rho_e})$	7.57

2.2. Laminar Shear Model Box and Preparation of Model Soil

Boundary conditions and behaviors of the model box are important factors affecting the shaking table model test of an underground structure. In this study, a 3D laminar shear model box with adjustable stiffness independently developed by the research group was selected as the testing box. The container is composed of fifteen horizontal layers made of steel tubes, where one layer can move relatively to another in conformity to the deformation mode of soil deposits in the container. As the free movement of horizontal and vertical boundaries, the boundary effects can be eliminated. In addition, the reflection effect of the box walls can be reduced by fixing rubber pads on both sides of the inside walls of the container. The previous experimental results show that the model box can not only meet the dynamic model test conditions of the underground structure but can also eliminate the boundary effect [30]. The soil container used in the test is shown in Figure 2.

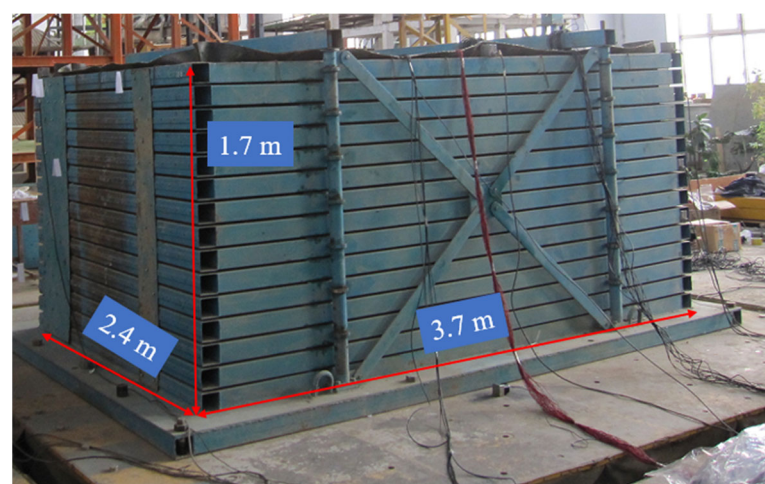


Figure 2. Laminar shear model box.

The river sand obtained from Harbin city was adopted for the soil model. Figure 3 shows the soil particle size distribution curve. The testing sand site was constructed layer by layer, and the total thickness of the ground soil was 1.2 m. The thickness of the overlying water on the sand soil was 0.2 m. The ground soil was fully saturated by water injection

pipes embedded in the sand ground. After saturation, the density of the testing sand was 1.98 g/cm^3 .

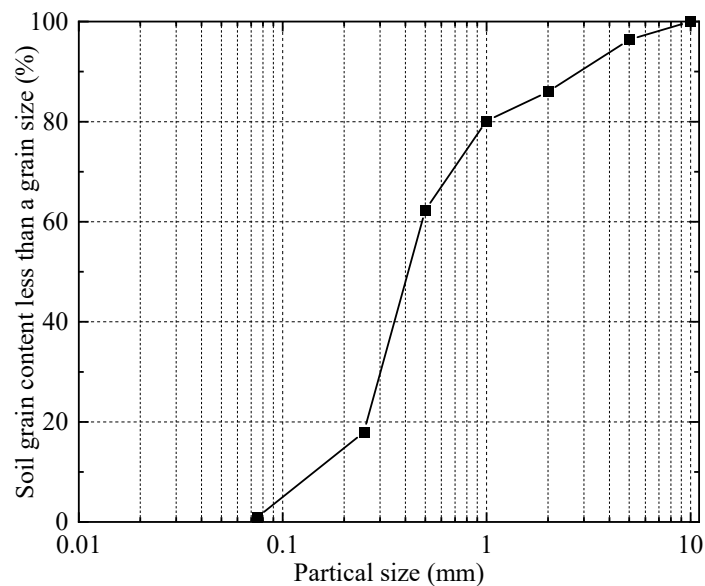


Figure 3. Particle size distribution curve.

2.3. Manufacture of Structural Model

Based on the particle–concrete mix ratio obtained from the laboratory test (cement 42.5#, water, sand–lime particle–concrete mixing proportion of 1.0:0.5:5.0:0.6), the structural model of the underground tunnel structure was made of particle–concrete. The tunnel model can be seen in Figure 4, with a length of 1800 mm, width of 1260 mm, height of 380 mm, and thickness of 50 mm. Galvanized mesh was used to simulate the embedded steel cage of the underground tunnel structure, and the tunnel model was completed by pouring and vibrating at one time for the purpose of ensuring the stiffness of the whole structure was consistent and uniform. Considering the structural inertial force, an artificial mass model was adopted. Eight lead counterweight blocks (each lead counterweight block weighs 50 kg) were applied to the top plate of the tunnel structure. Simultaneously, twelve lead counterweight blocks (each lead counterweight block weighs 25 kg) were arranged at both the left and right caverns of the bottom plate. The whole model system is shown in Figure 5.

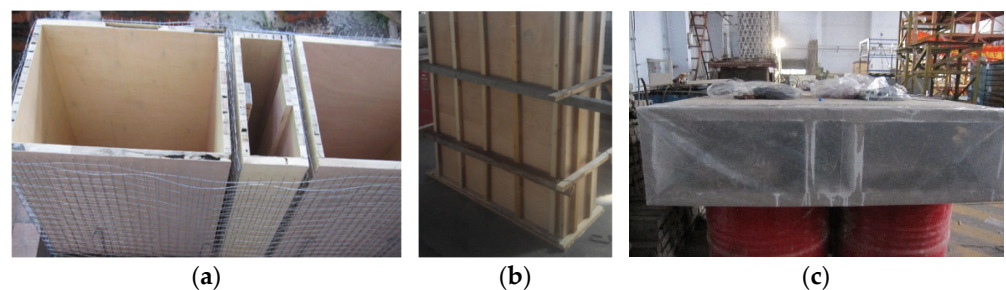


Figure 4. Design and fabrication of the underground structure model: (a) template and steel wire, (b) whole template, and (c) tunnel model.

2.4. Sensor Arrangement

The physical quantities include soil acceleration, strain of the model structure, and excess pore water pressure. To better obtain the experimental data, the main observation surface was set along the longitudinal center of the tunnel structure. In this paper, the accelerometer (measurement accuracy: $\pm 0.15\%$, ranges from -2 to 2 g), strain gauge

(measurement accuracy: $\pm 0.1\%$, ranges from $-20,000$ to $20,000 \mu\epsilon$), and pore pressure transducer (measurement accuracy: $\pm 0.1\%$, ranges from -100 to 100 kPa) were adopted during the supervision process, and for convenience, their abbreviations were labeled A, S, and P, respectively. The sensors' arrangement is introduced in Figure 6.

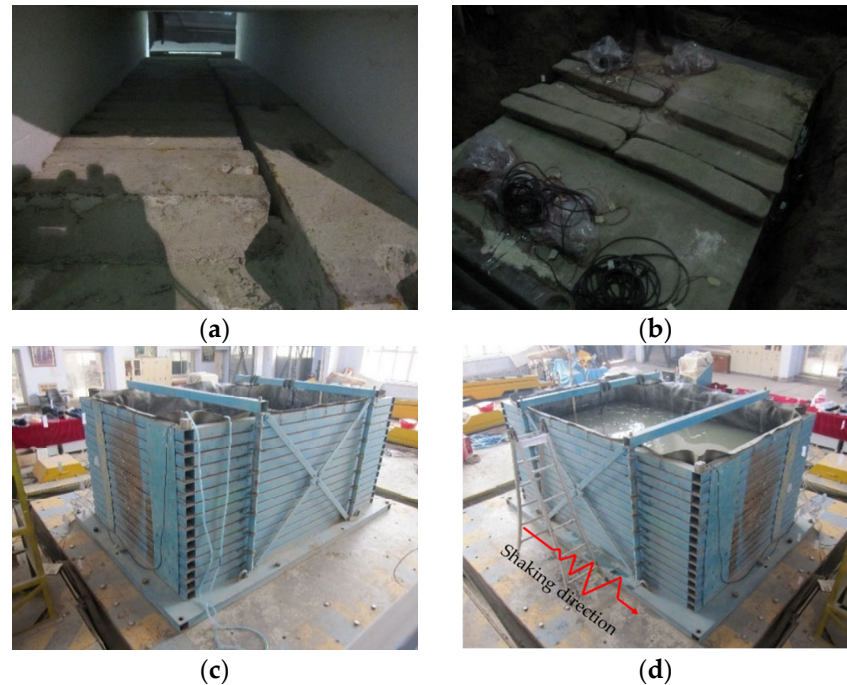


Figure 5. Assembly of model system: (a) counterweight set on the bottom plate, (b) counterweight set on the top plate, (c) water injection, and (d) final model system.

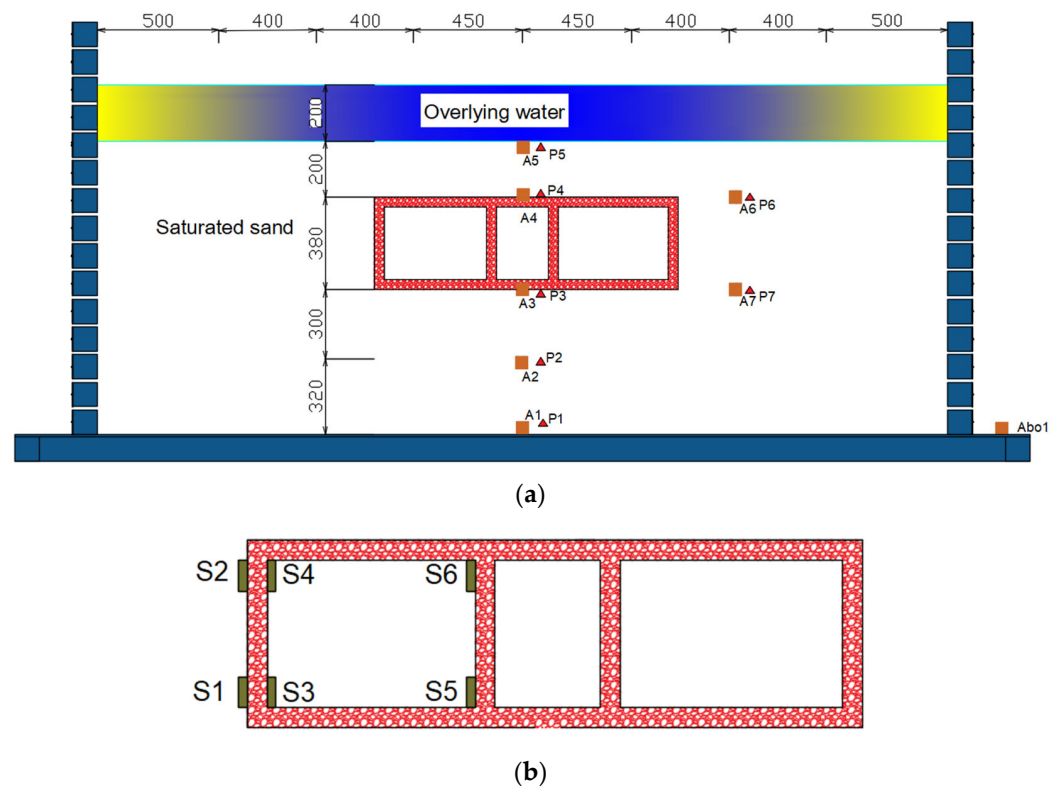


Figure 6. Sensor arrangement: (a) layout of the acceleration and water pore pressure sensors, and (b) layout of the structural strain gauges.

2.5. Input Earthquake Ground Motions

The El-Centro, Kobe, and Wolong earthquake acceleration records were selected as prototype excitations, of which the peak ground acceleration (PGA) values and time histories of the seismic motions were compressed and adopted as the testing earthquake inputs. According to the similarity relations listed in Table 1, the duration of the seismic excitations was 1/4 of the original seismic records. The three earthquake acceleration records and corresponding Fourier spectra are shown in Figure 7. The PGA values were adjusted to 0.1, 0.2, and 0.4 g for the small, moderate, and strong earthquake excitations, respectively. The earthquake input is in the longitudinal (X) direction. The input sequence of ground motions is El-Centro PGA 0.1 g, Kobe PGA 0.1 g, Wolong PGA 0.1 g, El-Centro PGA 0.2 g, Kobe PGA 0.2 g, Wolong PGA 0.2 g, El-Centro PGA 0.4 g, Kobe PGA 0.4 g, and Wolong PGA 0.4 g.

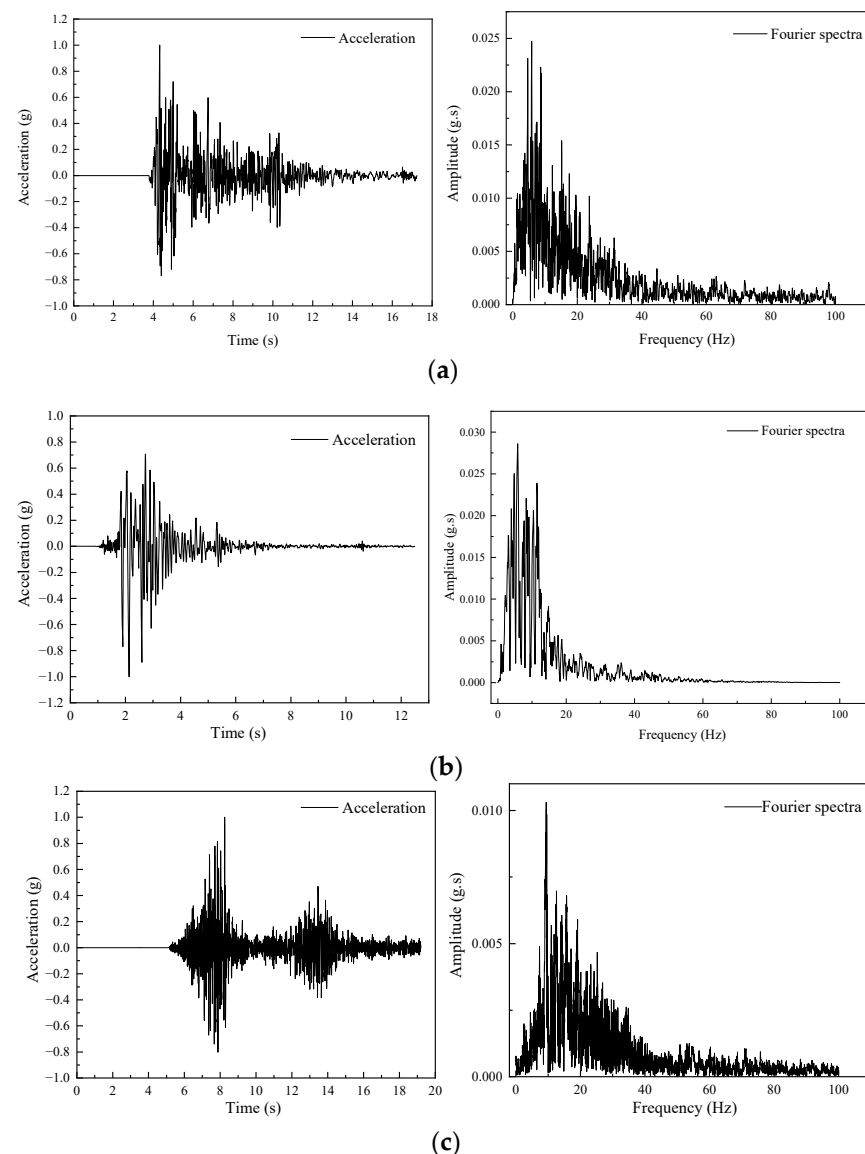


Figure 7. The acceleration time history curves and Fourier spectra of seismic excitation: (a) El-Centro, (b) Kobe, and (c) Wolong.

3. Testing Results and Analysis

The devolvement mechanism of excess pore water pressure, hysteretic characteristics of soil deposits, and peak strain of the underground structure model are the indispensable contents during the soil structure analysis program.

3.1. Excess Pore Water Pressure Ratio

The excess pore water pressure in the soil layer often rises rapidly under the action of obvious ground motion. For the investigation of the seismic behavior of the saturated sand in the underwater environment, evaluation of the excess pore water pressure ratio is necessary. The excess pore water pressure ratio, namely the ratio of excess pore water pressure to soil effective stress, can be used to identify the development trend of excess pore water pressure and effective stress. To facilitate the analysis, the excess pore water pressure ratios of water pore pressure sensors P2 and P4, which were embedded in the soil deposits underneath and upon the underground tunnel model, when subjected to 0.4 g Kobe and Wolong earthquake motions were selected to analyze. It should be noted that in these cases, the next loading condition should not be conducted until the soil reaches a stable state with a decline of the excess pore water pressure. Thus, the duration of the excess pore water pressure ratio record is longer than that of the input ground motion, as shown in Figure 8.

- (1) With respect to the time history curve of the excess pore water pressure ratio, a trend that the excess pore water pressure ratio decreases with the increase of the buried depth has been found. This is mainly due to the subsidiary stress caused by the dead weight of the underground tunnel model. Due to the effects of the existing subsidiary stress, the soil underneath the bottom plate is more compact than the soil above the tunnel structure.
- (2) Under the same input ground motion, the excess pore water pressure of the overburden soil layer above the tunnel structure dissipates faster than that of the soil layer underneath the tunnel structure, indicating that the existence of the underground structure can change the dissipation rate of the excess pore water pressure of soil.
- (3) From the point of view of the peak excess pore water pressure ratio value, the peak value under the Kobe excitation is larger than that under the Wolong excitation. Considering the Wolong ground motion, the proportion of high-frequency components is obvious. On the contrary, as for the Kobe ground motion, the low-frequency components are more abundant. It can be seen that the spectral characteristics of ground motion have a noticeable effect on the development of excess pore water pressure in saturated sand soil, which verifies the opinion introduced in [3].

3.2. Dynamic Shear Stress–Displacement Hysteretic Curves of Soil Deposits

Given that the shear horizontal earthquake wave propagates vertically in horizontal-stratified soil, the 1D shear beam method should always be adopted to the simplified model of the sand soil profile. According to the method introduced in [3], the shear stress history records as well as displacement can be calculated from the obtained seismic acceleration, and thus the dynamic shear stress–displacement hysteretic curves of soil can be acquired (the calculation diagram is introduced in Figure 9). The shear stress of the soil deposit at a buried depth, h , can then be denoted via the soil density, ρ , and the acceleration, a_z , at a buried depth, z , as $T(h, z) = \int_0^h \rho a_z dz$. Then, if the acceleration responses of different soil nodes (numbered in Figure 9) are obtained, the shear stress at any buried depths can be calculated. The calculation formula of dynamic shear stress for the inversion process is as follows:

$$T(z_i, t) = T(z_{i-1}, t) + \rho \frac{a(z_{i-1}, t) + a(z_i, t)}{2} \Delta z_{i-1} \quad (1)$$

where z_i denotes the soil body at a certain depth, t denotes time, Δz_i denotes the elevation difference of adjacent soil layers, ρ denotes the soil density, $a(z_i, t)$ denotes the acceleration of the z_i soil layer at time t , and $a(z_{i-1}, t)$ denotes the acceleration of the z_{i-1} soil layer at time t .

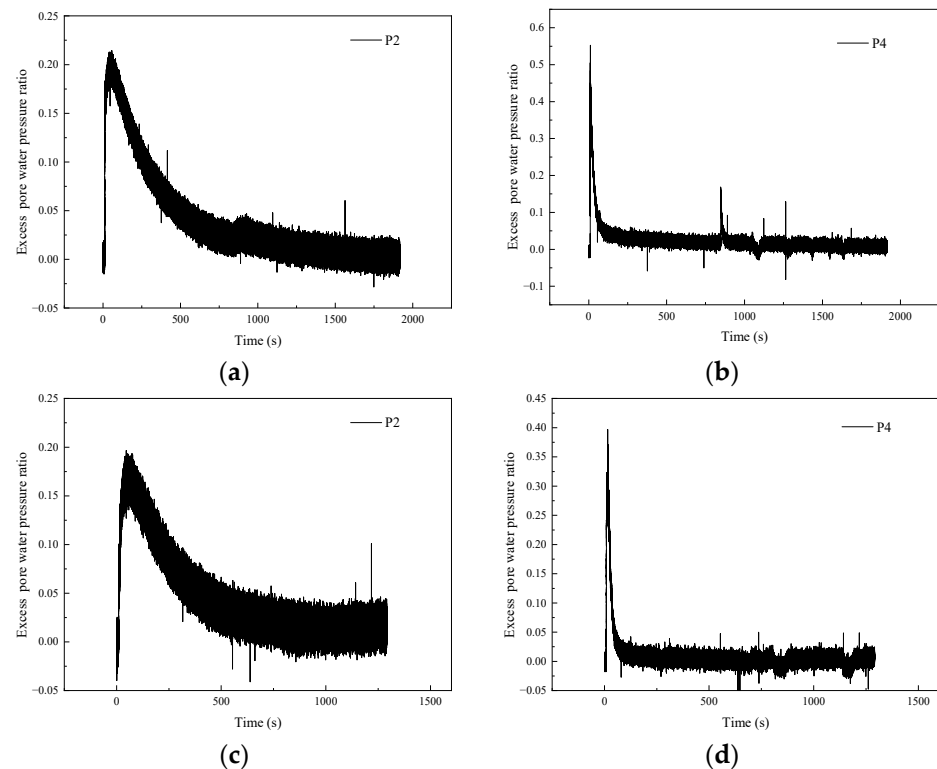


Figure 8. Excess pore water pressure ratio: (a) Kobe soil deposit with buried depth of 0.88 m, (b) Kobe soil deposit with buried depth of 0.2 m, (c) Wolong soil deposit with buried depth of 0.88 m, and (d) Wolong soil deposit with buried depth of 0.2 m.

Based on the measured acceleration time history records of the soil at different buried depths, the development law of shear stress of the sand soil can then be retrieved by means of integral iteration. The development of soil's shear stress of the top and bottom of the underground structure can be deduced from the testing accelerations, i.e., A5, A4, A3, and A2. The shear stress–displacement hysteretic curves of soil with buried depths of 0.2, 0.58, and 0.88 m are exhibited in Figure 10. Overall, the shear stress–displacement hysteretic curve is symmetrical, and the shear stress oscillates following the displacement direction of the soil.

- (1) From the perspective of the development trend of shear stress from soil layers with different buried depths, the shear stress of shallow buried soil is generally smaller than that of deep buried soil. The displacement of soil decreases with the increase of the buried depth, and the displacement of shallow buried soil is the largest. This is owing to the fact that the greater the buried depth, the larger the additional stress of soil. In addition, due to the existence of the underground tunnel model, the soil surrounding and below the tunnel structure is well-constrained.
- (2) Considering the loading case of 0.1 g of ground motion, since the input seismic energy of the ground is small, the soil deposits basically remain in an elastic state. A trend whereby different earthquake waves have little influence on the shear stress value of the soil deposits has been found. Otherwise, input the same PGA, and different ground motions imposed to the testing model system obviously significantly affect the shear stress of the soil deposits. Given the case of a loading level with PGA 0.4 g, the peak shear stress values of the soil deposits are -2.3 , -1.8 , and -0.9 kPa, respectively, corresponding to the excitations of El-Centro, Kobe, and Wolong ground motions. Particularly worth mentioning is that the spectrum characteristics of ground motions have a significant effect on the development law of shear stress under moderate and strong earthquakes.

- (3) Ground motions have significant influence on the displacement of soil deposits. Taking the displacement of the soil deposit with a buried depth of 0.2 m for instance, under different seismic excitations with the same PGA, El-Centro ground motion induces the largest displacement, followed by the Kobe ground motion, and finally the Wolong ground motion, and the difference is more obvious when the input PGA is larger. This is mainly due to effects of ground motions on the dynamic responses of the saturated sandy soil site, i.e., the excess pore water pressure increases rapidly, which has the characteristic of filtering the high-frequency component of seismic waves, and thus the low-frequency portion plays a more obvious role.
- (4) With respect to the shear stress–displacement hysteretic curve, the hysteretic loop of each soil layer shows a good regularity in general under the loading cases of 0.1 g ground motions. The hysteretic loops become steeper with the increase of soil displacement. When the input PGA increases to 0.2 and 0.4 g, the hysteretic loop gradually slows down with the increase of soil displacement, and the area formed by the hysteretic loop expands. There is accumulating plastic deformation of soil deposits showing a softening trend and indicating that the nonlinear characteristics of the soil deposits are pretty obvious. Furthermore, there is an apparent attenuation law observed from the shear stiffness (namely the diagonal slope of a hysteretic loop) of the soil deposit with a buried depth of 0.2 m, followed by the soil deposit with a buried depth of 0.58 m. This phenomenon is not obvious in the soil deposit with a buried depth of 0.58 m. The development law of soil deposits' shear stiffness can be explained in two aspects. On the one hand, the stiffness of the underground structure is large, which better restricts the deformation of the bottom soil. On the other hand, the excess pore water pressure of saturated sand at a shallow depth increases faster than that at a deep depth, and the effective stress of soil decreases more obviously; thus, the soil is more likely to produce and accumulate plastic deformation during the earthquake process.

Previous studies have generally focused on the shear stress–shear strain of the soil body, which cannot directly reflect the accumulated plastic deformation behavior. The shear stress–displacement hysteretic curve in this section can better express the accumulated plastic deformation capacity of the soil.

3.3. Equivalent Dynamic Horizontal Subgrade Reaction Coefficient

The dynamic response of underground structures is largely determined by the soil deformation during earthquake events. The subgrade reaction coefficient directly affects the distribution rule of the subsoil reaction field, which is also one of the decisive factors affecting the spring stiffness of ground soil during the analysis process of the seismic response of underground structures by using the response displacement method. In addition, the subgrade reaction coefficient can reflect the effect of the soil–structure interaction to a certain extent. In the past studies, the subgrade reaction coefficient was obtained only by static tests, and the results tended to be single; in that way, an obvious shortage often occurs during the analysis progress of the seismic response of underground structures. Based on the Winkler theory [31,32] and the idea of an equivalent subgrade reaction coefficient proposed in [33], the equivalent dynamic subgrade reaction coefficient can be obtained by estimating the slope of a typical hysteresis loop.

According to the shear stress–displacement hysteretic curves of soil deposits under different loading conditions in Section 3.2, a single loop at the time that the maximum and minimum displacements occur can be selected to measure the scope of the equivalent dynamic horizontal subgrade reaction coefficient. The shortcomings of the method introduced in [33] (which regards the slope of a typical hysteresis loop as the equivalent dynamic horizontal subgrade reaction coefficient) can then be covered. The maximum horizontal equivalent dynamic subgrade reaction coefficients are listed in Table 2, which indicates that:

- (1) The equivalent dynamic horizontal subgrade reaction coefficient increases with the increase of the buried depth. The difference between the equivalent dynamic horizontal subgrade reaction coefficient above and underneath the underground structure model is the largest. Considering the loading case of the 0.1 g El-Centro ground motion, the difference reaches 7.589 MN/m^3 .
- (2) The equivalent dynamic horizontal subgrade reaction coefficient decreases with the increase of the input PGA, especially under the action of moderate and strong earthquakes. The maximum reduction ratios of the equivalent dynamic horizontal subgrade reaction coefficient are 74.4%, 66.7%, and 47.3%, corresponding to the El-Centro, Kobe, and Wolong ground motions, respectively.
- (3) Comparing the maximum equivalent dynamic horizontal subgrade reaction coefficients of soil deposits under three ground motions, there are certain differences among the coefficients of the soil deposit with the same buried depth when subjected to the same input PGA. Under the loading conditions with 0.1 g PGA, the coefficient values of the loading case of El-Centro waves are generally larger than those of the other two seismic excitations. Owing to the order of input ground motions (El-Centro ground motion first, then Kobe ground motion, and finally Wolong ground motion), the soil remains in the initial state before the input of the El-Centro ground motion. When PGA increases to 0.2 and 0.4 g, the coefficient values of the loading case of the El-Centro wave are generally smaller than those of the other two seismic excitations. This may be because the low-frequency components of the El-Centro record are more abundant than the other two ground motions. Under the action of moderate and strong earthquakes, the liquefaction degree of saturated sand soil is increased, in which the influence of the low-frequency components of ground motion must be amplified. It also supports the opinion that the degree of liquefaction can affect the dynamic response of site soil [20].

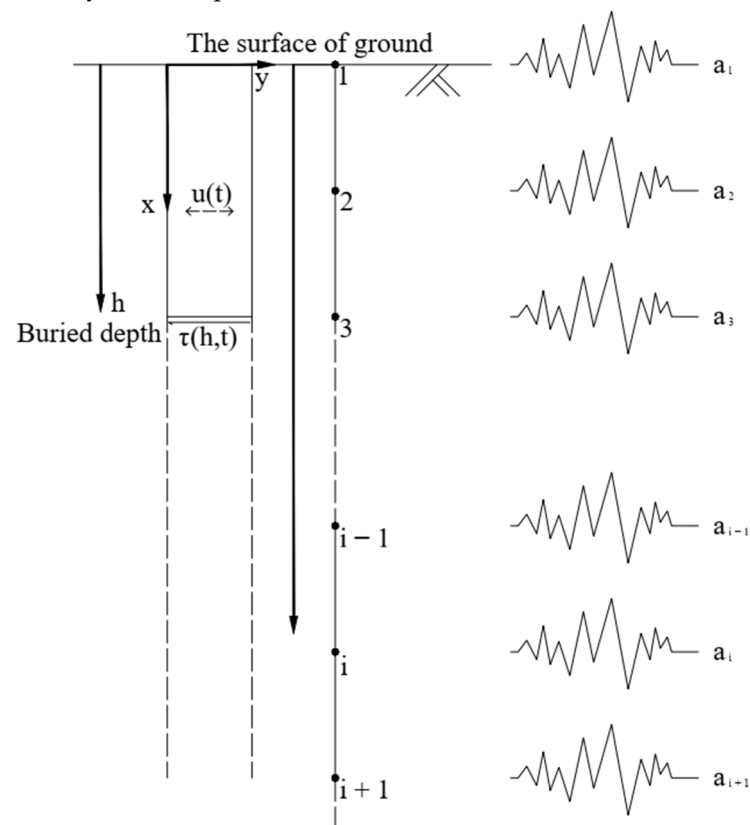


Figure 9. 1D shear beam method.

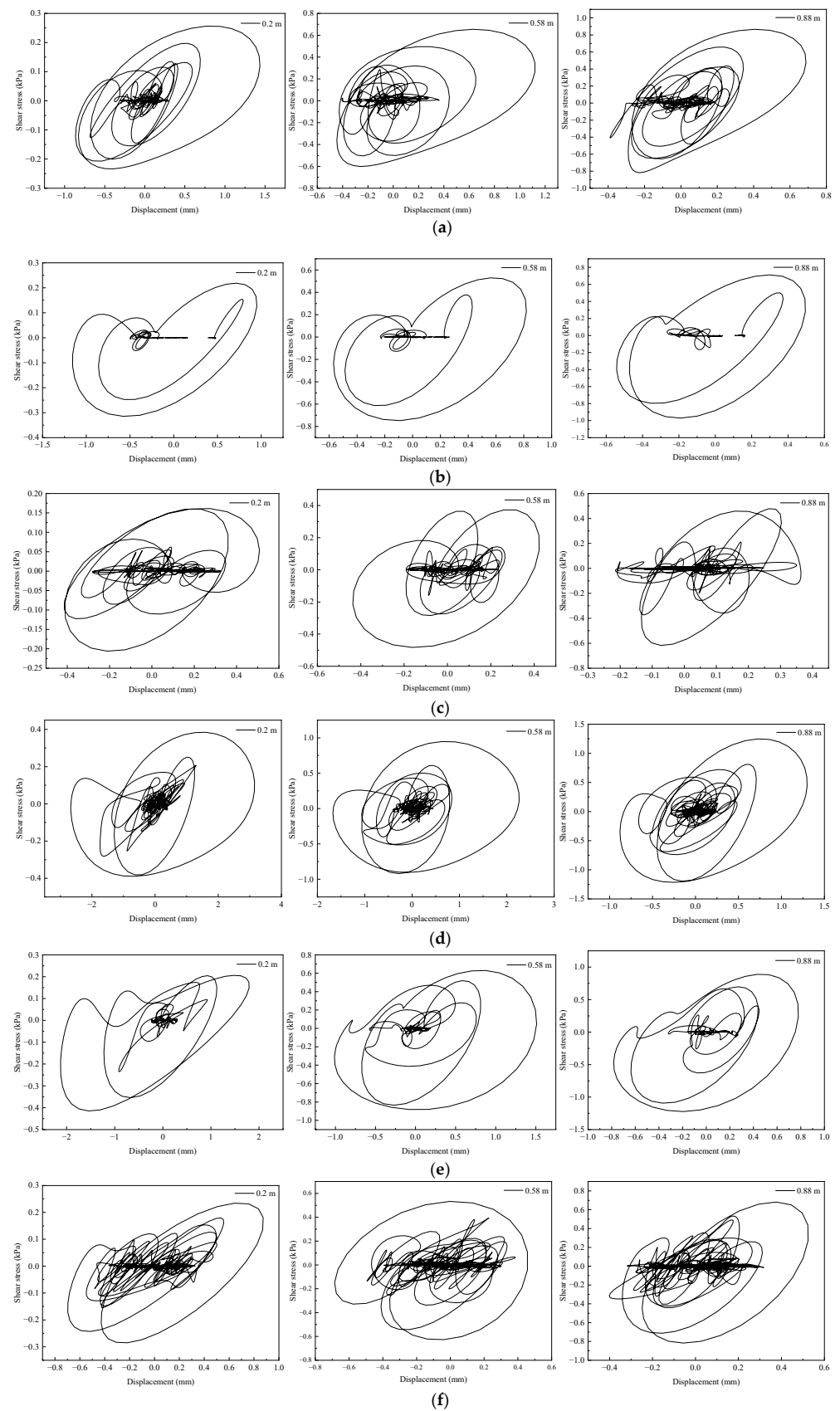


Figure 10. Cont.

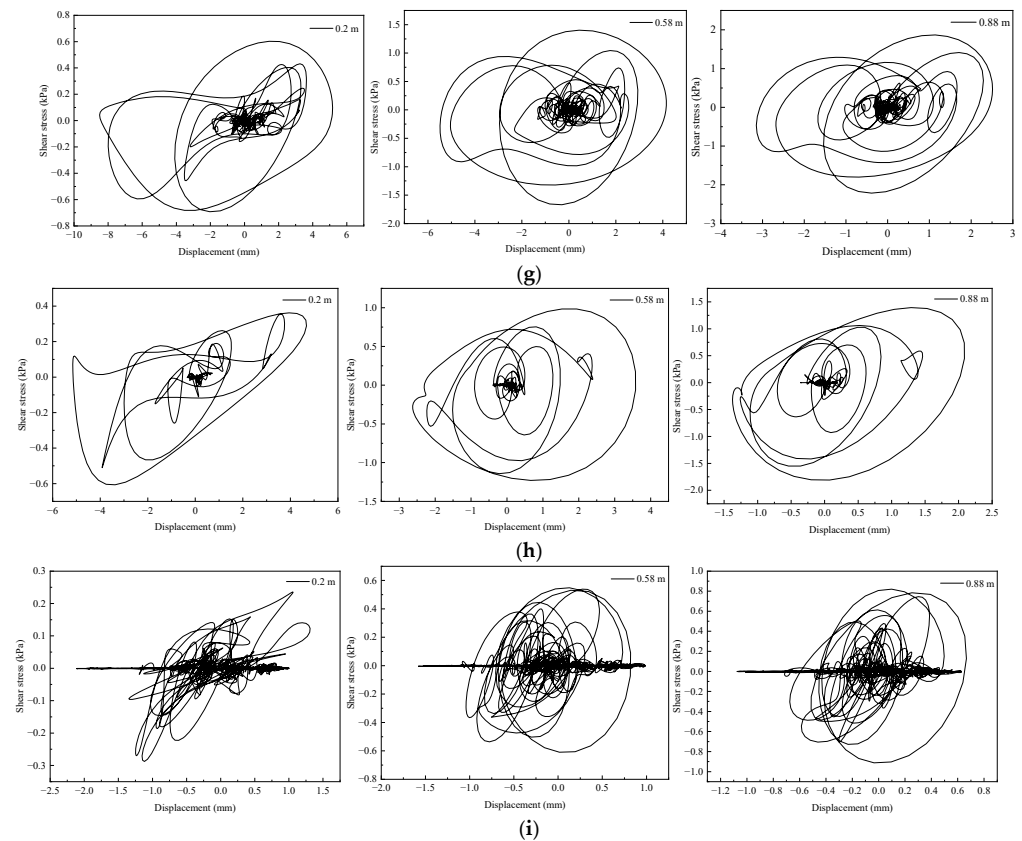


Figure 10. Shear stress–displacement hysteretic curves: (a) El-Centro 0.1 g, (b) Kobe 0.1 g, (c) Wolong 0.1 g, (d) El-Centro 0.2 g, (e) Kobe 0.2 g, (f) Wolong 0.2 g, (g) El-Centro 0.4 g, (h) Kobe 0.4 g, and (i) Wolong 0.4 g.

Table 2. The maximum equivalent dynamic horizontal subgrade reaction coefficients (unit: MN/m^3): B.D. denotes the buried depth of soil deposits.

PGA	El-Centro Ground Motion			Kobe Ground Motion			Wolong Ground Motion		
	B.D. 0.2 m	B.D. 0.58 m	B.D. 0.88 m	B.D. 0.2 m	B.D. 0.58 m	B.D. 0.88 m	B.D. 0.2 m	B.D. 0.58 m	B.D. 0.88 m
0.1 g	0.617	7.716	8.206	0.744	3.667	5.772	0.764	3.348	5.799
0.2 g	0.442	2.110	4.721	0.413	3.496	5.092	0.855	2.947	4.966
0.4 g	0.353	1.983	3.552	0.248	2.570	3.986	0.503	2.625	3.051

3.4. Dynamic Strain of the Underground Structure Model

The dynamic strain variation law of the underground structure model can reflect the stress variation characteristics of the underground structure model to a certain extent. According to the recorded data of strain gauges S1 and S2 at both ends of the left wall, the corresponding dynamic strain can be obtained by zeroing and baseline correction. As Figure 11 shows:

- (1) Under all loading conditions, the strain on the sidewall of the underground structure presents the characteristics of approximate symmetry in tension and compression directions. In general, the peak dynamic strain value at the top of the sidewall is higher than that at the bottom of the sidewall (i.e., under the loading condition of El-Centro PGA 0.1 g, the peak dynamic strains of the top and bottom of the sidewall are 22.5 and $-18.1 \mu\epsilon$, respectively), and this is similar to the distribution law of shear displacement in the soil deposits, which also coincides with the law that the seismic response of underground structures is controlled by the soil deformation.
- (2) The peak dynamic strain of the underground structure increases with the increase of the seismic excitation amplitude. The increase of the dynamic strain value of the

top of the sidewall is obviously higher than that of the bottom of the sidewall when input PGA ranges from 0.1 to 0.2 g. Given that PGA of El-Centro ranges from 0.1 to 0.2 g, the compression (negative value in Figure 9) and tension (positive value in Figure 9) strain values of the top of the sidewall increase by 17.2 and 8.5 $\mu\epsilon$, while those of the bottom of the sidewall increase by 3.2 and 8.4 $\mu\epsilon$. The same rule has also been found under the other two seismic excitations. While, in the case of the same PGA, the peak dynamic strains are different due to different ground motions, i.e., the peak dynamic strain values of the top of the sidewall under the loading conditions of El-Centro PGA 0.2 g, Kobe PGA 0.2 g, and Wolong PGA 0.2 g are -38.7 , -33.7 , and 30.7 $\mu\epsilon$, respectively. With the increase of PGA, the displacement of the soil deposit above the underground structure is significantly greater than that of the soil deposit surrounding and underneath the underground structure, and the equivalent dynamic horizontal subgrade reaction coefficient of the soil deposits also begins to decline. Thus, the elastic resistance of the soil to the underground structure decreases. Consequently, the structure needs to resist more seismic energy. It is also verified that the buried depth of underground structures and the development of internal forces of soil deposits can directly affect the level of soil–underground structure interaction.

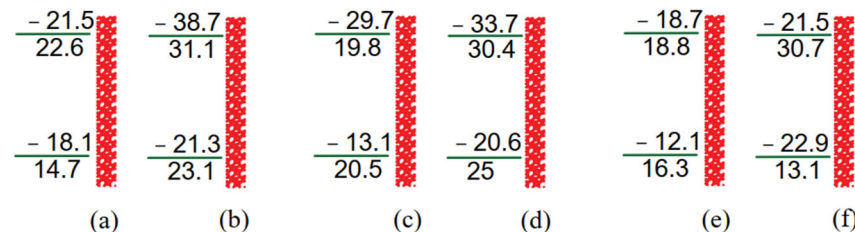


Figure 11. Peak dynamic strain of the sidewall in the underground structure: (a) El-Centro 0.1 g, (b) El-Centro 0.2 g, (c) Kobe 0.1 g, (d) Kobe 0.2 g, (e) Wolong 0.1 g, and (f) Wolong 0.2 g.

4. Conclusions and Discussions

4.1. Discussion

The estimation of the seismic performance of liquefiable sand sites and underground structures is meaningful. The findings of this study can provide novel insight to analyze the dynamic behavior of saturated sand deposits. The evaluation method of the equivalent dynamic horizontal subgrade reaction coefficient proposed by this study can reflect the actual relationship between the subgrade restraint and the soil buried depth, which may cover the shortcomings of the previous method. Furthermore, the application of the equivalent dynamic horizontal subgrade reaction coefficient method can better improve the calculation accuracy of the spring stiffness value during the anti-seismic design of underground structures by using the response displacement method.

The following aspects are recommended for further research:

- (1) More case studies about actual underground tunnels embedded in soft soil sites under seismic motions are required.
- (2) Numerical models investigating the saturated soil–underground structure interaction under diverse earthquake loadings are necessary.
- (3) High-precision sensors as well as mathematic methods estimating the seismic performance of soil foundations and underground structures need further development.

4.2. Conclusions

The present study introduced detailed information about the shaking table test of a saturated sand–underground structure system. Based on the testing results, the development law of the excess pore water pressure ratio, the variation mechanism of shear stress–displacement hysteretic curves, the equivalent dynamic horizontal subgrade reaction coefficient, and the peak dynamic strain values of the underground structure were analyzed and discussed, and the main conclusions were drawn as follows:

- (1) In consideration of the shaking process, the shear stress of the soil deposit above the underground structure and the soil deposits on both sides of the underground structure was smaller than that of the sand deposit underneath the underground structure, while the distribution law of the soil displacement showed the opposite trend (the shear stress–displacement hysteretic curves of the testing soil deposits exhibited that the shear stress of the soil deposits with a buried depth of 0.88 m was the largest, while the horizontal displacement was the smallest). The underground tunnel structure improved the additional effective stress of the ground soil to a certain extent.
- (2) The spectral characteristics of ground motion had obvious effects on the soil deformation of saturated sandy soil, especially when exposed to moderate and strong earthquakes. Inputting the ground motion with rich low-frequency components, the shear stress–displacement hysteretic loop of soil was plump, and the accumulated plastic deformation of soil deposits was obvious.
- (3) A certain degree of softening phenomenon of soil can be reflected by the shear stress–displacement hysteretic curves, which can be properly related to the horizontal displacement of the soil deposits and generation of the excess pore water pressure.
- (4) Based on the shear stress–displacement hysteretic curves of soil deposits, the equivalent dynamic horizontal subgrade reaction coefficient can be obtained by calculating the ratio of shear stress to displacement at any time in the earthquake time histories. The horizontal equivalent dynamic subgrade reaction coefficient increased with the increase of the soil buried depth and decreased with the increase of the input PGA value.
- (5) In the case of small earthquakes, the order of the input ground motions can affect the value of the equivalent dynamic horizontal subgrade reaction coefficient. While in the case of moderate and strong earthquakes, soil liquefaction can influence the equivalent dynamic horizontal subgrade reaction coefficient.
- (6) The peak dynamic strain value of the top of the sidewall was higher than that of the bottom of the sidewall when subjected to earthquakes. Overall, the development law of structural dynamic strain was in good agreement with the displacement distribution pattern of the soil deposits. Special attention should be paid to observing the foundation deformation underneath underground structures, as well as estimation of the shear stress state of the soil deposits on both sides and above underground structures. In extreme cases, corresponding measures should be taken to reduce the stress of underground structures buried in saturated sand sites.
- (7) This paper is a part of the results of the soil-underground structure shaking table model test. It is also worth analyzing the effects of soil materials and underground structure types on the seismic responses of underground structures. In addition, further improvements on the understanding of the seismic capacity of underground structures and related references for the earthquake prevention and disaster reduction of underground structures are also worth exploring.

Author Contributions: Conceptualization and design, X.C. and L.J.; methodology, X.C., Z.H., L.J. and J.C.; simulation and data collection, X.C. and X.X.; data curation, X.C. and H.L.; writing—review and editing, X.C.; funding acquisition, X.C. and J.C. All authors have read and agreed to the published version of the manuscript.

Funding: This research was funded by the funding support from the Scientific Research Fund of the State Key Laboratory of Mechanical Behavior and System Safety of Traffic Engineering Structures, Shijiazhuang Tiedao University (Grant No. KF2020-20), and the National Natural Science Foundation of China (NSFC) (Grant Nos. 52008081, 52168045, and 52020105002).

Data Availability Statement: Not applicable.

Conflicts of Interest: The authors declare no conflict of interest.

References

- Wang, J.N.; Yang, J.; Zhuang, H.Y.; Ma, G.; Sun, Y. Seismic responses of a large unequal-span underground subway station in liquefiable soil using shaking table test. *J. Earthq. Eng.* **2021**, *11*, 1–22. [\[CrossRef\]](#)
- Zhao, K.; Wang, Q.Z.; Chen, Q.; Zhuang, H.Y.; Chen, G.X. Simplified effective stress modeling of shear wave propagation in saturated granular soils. *Geotech. Lett.* **2021**, *11*, 1–9. [\[CrossRef\]](#)
- Ko, Y.Y.; Chen, C.H. On the variation of mechanical properties of saturated sand during liquefaction observed in shaking table tests. *Soil Dyn. Earthq. Eng.* **2020**, *129*, 105946. [\[CrossRef\]](#)
- Chattaraj, R.; Sengupta, A. Liquefaction potential and strain dependent dynamic properties of Kasai River sand. *Soil Dyn. Earthq. Eng.* **2016**, *90*, 467–475. [\[CrossRef\]](#)
- Ye, B.; Xie, X.; Zhao, T.; Song, S.; Ma, Z.; Feng, X.; Zou, J.; Wang, H. Centrifuge tests of macroscopic and mesoscopic investigation into effects of seismic histories on sand liquefaction resistance. *J. Earthq. Eng.* **2020**, *26*, 4302–4324. [\[CrossRef\]](#)
- Xie, X.L.; Ye, B.; Zhao, T.; Feng, X.Q.; Zhang, F. Changes in sand meso-structure under repeated seismic liquefaction events during centrifuge tests. *Soil Dyn. Earthq. Eng.* **2021**, *150*, 106940. [\[CrossRef\]](#)
- Shooshpasha, I.; Bagheri, M. The effects of surcharge on liquefaction resistance of silty sand. *Arab. J. Geosci.* **2014**, *7*, 1029–1035. [\[CrossRef\]](#)
- Hamada, M.; Isoyama, R.; Wakamatsu, K. Liquefaction-induced ground displacement and its related damage to lifeline facilities. *Soils Found.* **1996**, *36*, 81–97. [\[CrossRef\]](#)
- Uenishi, K.; Sakurai, S. Characteristic of the vertical seismic waves associated with the 1995 Hyogo-ken Nanbu (Kobe), Japan earthquake estimated from the failure of the Daikai Underground Station. *Earthq. Eng. Struct. Dyn.* **2000**, *29*, 813–821. [\[CrossRef\]](#)
- Tokimatsu, K.; Tamura, S.; Suzuki, H.; Katsumata, K. Building damage associated with geotechnical problems in the 2011 Tohoku Pacific Earthquake. *Soils Found.* **2012**, *52*, 956–974. [\[CrossRef\]](#)
- Yamaguchi, A.; Mori, T.; Kazama, M.; Yoshida, N. Liquefaction in Tohoku district during the 2011 off the Pacific Coast of Tohoku Earthquake. *Soils Found.* **2012**, *52*, 811–829. [\[CrossRef\]](#)
- Wang, W.L.; Wang, T.T.; Su, J.J.; Lin, C.H.; Seng, C.R.; Huang, T.H. Assessment of damage in mountain tunnels due to the Taiwan Chi-Chi earthquake. *Tunn. Undergr. Space Technol.* **2001**, *16*, 133–150. [\[CrossRef\]](#)
- Zhuang, H.; Hu, Z.; Wang, X.; Chen, G. Seismic responses of a large underground structure in liquefied soils by FEM numerical modelling. *Bull. Earthq. Eng.* **2015**, *13*, 3645–3668. [\[CrossRef\]](#)
- Chen, S.; Wang, X.; Zhuang, H.; Xu, C.; Zhao, K. Seismic response and damage of underground subway station in a slightly sloping liquefiable site. *Bull. Earthq. Eng.* **2019**, *17*, 5963–5985. [\[CrossRef\]](#)
- Zhao, K.; Zhu, S.D.; Bai, X.X.; Wang, Q.; Chen, S.; Zhuang, H.; Chen, G. Seismic response of immersed tunnel in liquefiable seabed considering ocean environmental loads. *Tunn. Undergr. Space Technol.* **2021**, *115*, 104066. [\[CrossRef\]](#)
- Liang, L.; Hongyun, J.; Xiuli, D.; Peixin, S. Fully fluid-solid coupling dynamic model for seismic response of underground structures in saturated soils. *Earthq. Eng. Eng. Vib.* **2020**, *19*, 257–268. [\[CrossRef\]](#)
- Li, L.; Shi, P.X.; Du, X.L.; Jiao, H. Using numerical simulation to determine the seismic response of coastal underground structures in saturated soil deposits. *J. Coastal Res.* **2017**, *33*, 583–595. [\[CrossRef\]](#)
- Yu, H.T.; Yan, X.; Bobet, A.; Yuan, Y.; Xu, G.; Su, Q. Multi-point shaking table test of a long tunnel subjected to non-uniform seismic loadings. *Bull. Earthq. Eng.* **2018**, *16*, 1041–1059. [\[CrossRef\]](#)
- Yu, H.T.; Yuan, Y.; Xu, G.P.; Su, Q.; Yan, X.; Li, C. Multi-point shaking table test for long tunnels subjected to non-uniform seismic loadings—Part II: Application to the HZM immersed tunnel. *Soil Dyn. Earthq. Eng.* **2018**, *108*, 187–195. [\[CrossRef\]](#)
- Ding, X.M.; Zhang, Y.L.; Wu, Q.; Chen, Z.; Wang, C. Shaking table tests on the seismic responses of underground structures in coral. *Tunn. Undergr. Space Technol.* **2021**, *109*, 103775. [\[CrossRef\]](#)
- Kheradi, H.; Nagano, K.; Nishi, H.; Zhang, F. 1-g shaking table tests on seismic enhancement of existing box culvert with partial ground-improvement method and its 2D dynamic simulation. *Soils Found.* **2018**, *58*, 563–581. [\[CrossRef\]](#)
- Su, C.; Baizan, T.; Haiyang, Z.; Jianning, W.; Xiaojun, L.; Kai, Z. Experimental investigation of the seismic response of shallow-buried subway station in liquefied soil. *Soil Dyn. Earthq. Eng.* **2020**, *136*, 106153. [\[CrossRef\]](#)
- Tao, L.J.; Shi, C.; Deng, P.; Zhang, F. Shaking table test of the effect of an enclosure structure on the seismic performance of a prefabricated subway station. *Tunn. Undergr. Space Technol.* **2022**, *125*, 104533. [\[CrossRef\]](#)
- Koseki, J.; Matsuo, O.; Koga, Y. Uplift behavior of underground structures caused by liquefaction of surrounding soil during earthquake. *Soils Found.* **1997**, *37*, 97–108. [\[CrossRef\]](#)
- Zhu, T.; Wang, R.; Zhang, J.M. Evaluation of various seismic response analysis methods for underground structures in liquefiable ground. *Tunn. Undergr. Space Technol.* **2021**, *110*, 103803. [\[CrossRef\]](#)
- Mahmoud, A.O.; Hussien, M.N.; Karray, M.; Chekired, M.; Bessette, C.; Jinga, L. Mitigation of liquefaction-induced uplift of underground structures. *Comput. Geotech.* **2020**, *125*, 103663. [\[CrossRef\]](#)
- Zhang, M.Z. Study on similitude laws for shaking table tests. *Earthq. Eng. Eng. Vib.* **1997**, *2*, 52–58. (In Chinese)
- Chen, H.J.; Li, X.J.; Yan, W.M.; Chen, S.; Zhang, X. Shaking table test of immersed tunnel considering the geological condition. *Eng. Geol.* **2017**, *227*, 93–107. [\[CrossRef\]](#)
- Han, L.; Liu, H.L.; Zhang, W.A.; Ding, X.; Chen, Z.; Feng, L.; Wang, Z. Seismic behaviors of utility tunnel-soil system: With and without joint connections. *Undergr. Space* **2022**, *7*, 798–811. [\[CrossRef\]](#)

-
30. Sun, H.F.; Jing, L.P.; Meng, X.C.; Wang, N.W. A three-dimensional laminar shear soil container for shaking table test. *J. Vib. Shock* **2012**, *13*, 26–32. (In Chinese)
 31. David, Z.Y.; Moshe, E.; Moshe, A.A. Analysis of beams on nonlinear winkler foundation. *Comput. Struct.* **1989**, *31*, 287–292. [[CrossRef](#)]
 32. Pan, Y.J.; Li, G.S.; Liu, S.C.; Ouyang, T.J.; Cai, G.C. Study on the test method and value of the horizontal subgrade coefficient. *Chin. J. Undergr. Space Eng.* **2018**, *14*, 712–718. (In Chinese)
 33. Xu, K.; Jing, L.; Cheng, X.; Liang, H.; Bin, J. Laboratory tests for subgrade reaction coefficient in seismic design of underground engineering domain. *Adv. Civ. Eng.* **2020**, *10*, 1–14. [[CrossRef](#)]